Available online at www.sciencedirect.com
ScienceDirect
Polymer 49 (2008) 676–680
polymer
www.elsevier.com/locate/polymer

Polymer Communication

Early stages of polymer melt crystallization

P. Panine, E. Di Cola, M. Sztucki, T. Narayanan*

European Synchrotron Radiation Facility, F-38043 Grenoble, France

Received 14 October 2007; received in revised form 10 December 2007; accepted 11 December 2007
Available online 7 January 2008

Abstract

The early stage of crystallization of isotactic polypropylene was investigated by high brilliance X-ray scattering methods. The unprecedented detectivity allowed us to observe the appearance of crystalline nuclei prior to the onset of mesoscopic order. This observation is consistent with the nucleation and growth picture and excludes previously proposed spinodal-assisted mechanism of polymer crystallization. The early stage growth kinetics deviates from the empirical Avrami type description as suggested by cluster distribution models.

Keywords: Polypropylene; X-ray scattering; Isothermal crystallization

1. Introduction

Upon cooling the melt below the crystallization temperature, polymers rarely transform to a perfect crystal [1,2]. During the cooling process polymer chains cannot fully disentangle and only a part attains the favorable orientation for crystallization. As a result, the material turns into a metastable state consisting of crystalline and amorphous fractions [2]. This semi-crystalline nanostructure developed during the solidification process primarily controls the mechanical and physical properties of solid polymers. Therefore, the polymer crystallization has been a topic of both fundamental and practical interest over the past half century [1–4]. It has been well established that the transformation of an entangled melt into a semi-crystalline state involves multiple steps. Subsequent stage, commonly referred to as secondary crystallization, is largely described by phenomenological-type theories (e.g. Lauritzen–Hoffman) [5] but recent computer simulations have shed new light into the origin of lamellar structure in semi-crystalline polymers [3].

In contrast, the mechanism underlying the initial ordering process in melt crystallization has been a subject of debate [6,7]. X-ray scattering experiments have been widely used in the investigation of different facets of polymer crystallization [8–12]. Some of these experiments suggested the existence of crystallization precursors during the induction period [8,9,11]. The observed evolution of small-angle scattered intensity prior to the appearance of crystalline diffraction has been attributed to a signature of spinodal-like ordering process [8,9]. This small-angle scattered intensity was analyzed in terms of the Cahn–Hilliard (C–H) theory of phase ordering and the apparent linear behavior of C–H plot was attributed to the long-range density fluctuations associated with a spinodal-assisted ordering process [9,11]. However, this analysis has been questioned on the basis of the detection limit of X-ray scattering techniques to identify low level of crystalline content at the initial stages of crystallization [10]. The observed deviation from the classical picture of nucleation and growth has been rationalized in terms of experimental detection limit without the need to invoke additional mechanism such as spinodal decomposition [10,12,13]. Furthermore, transient intermediate states of smectic-like ordering of the polymer chains are often encountered in crystallization under extensional flows [14–16].

Similar differences in conclusion are also found in the modeling and simulation of early stage of polymer crystallization. The spinodal-assisted ordering process is rationalized on the basis of a metastable liquid–liquid phase boundary within the equilibrium liquid–crystal coexistence region, induced

* Corresponding author. Tel.: +33 4 76 88 21 21; fax: +33 4 76 88 24 25.
E-mail address: narayan@esrf.fr (T. Narayanan).

0032-3861/$ - see front matter © 2008 Elsevier Ltd. All rights reserved.
doi:10.1016/j.polymer.2007.12.026

by the coupling between density and chain conformation [7]. However, Langevin dynamics simulation of crystallization from solution and analytical model involving entropic frustration explained the above scattering experimental results on the basis of nucleation and growth type mechanism [3]. In addition, the computer simulation has illustrated an intermediate smectic-like order (involving oriented baby nuclei and the flexible strands linking them) prior to the emergence of folded chain structure. On the other hand, recent atomistic simulation provided evidence for spinodal-like liquid–liquid phase separation with nematic or smectic ordered domains and isotropic disordered regions [17]. Subsequent coarsening leads to crystalline and amorphous regions, respectively.

In order to disentangle these different scenarios of polymer crystallization, we have reinvestigated the early stage of crystallization in isotactic polypropylene (i-PP) using high brilliance small-angle and wide-angle X-ray scattering techniques (SAXS and WAXS, respectively). The unprecedented sensitivity and time resolution reached in this study allowed us to probe the time window upon reaching the isothermal condition and to monitor the corresponding structural changes at both molecular and mesoscopic length scales. In order to compare our results with previous investigations, we have used similar crystallization conditions and cooling rate as in those studies [9–11]. In addition, we have examined the ultra small-angle region that is not usually probed during the fast cooling and the so-called induction period.

2. Experimental section

The i-PP sample (Innovia Films, U.K.) had number (M_n) and weight (M_w) averaged molecular weights of 80,000 and 280,000 g/mol, respectively ($M_w/M_n \approx 3.5$, determined by melt flow index). This polymer sample (thickness $\approx$ 1 mm) was prepared without additives and the melting point (T_m) obtained from differential scanning calorimetry (DSC) was 165 °C (at a heating rate of 0.167 °C/s). In order to determine reproducible crystallization protocols, different experimental conditions such as the quench depth, annealing time of the melt and cooling rate were explored using a heating stage (Linkam, THMS600). The results presented here correspond to annealing at 210 °C for 300 s that is sufficient to remove all semi-crystalline history as verified by the melt scattering. To ensure good thermal contact between the sample and the heating stage, and to avoid direct contact with air, sample was encapsulated in thin aluminum foil of thickness <10 μm. These thin foils were carefully chosen such that their scattering contribution is much less than the i-PP melt scattering. As a result, the subtraction of aluminum foil scattering has not caused any problems in the SAXS region and the diffraction peaks of aluminum and i-PP are well separated and the powder rings of aluminum were physically masked on the WAXS detector. Moreover, the homogeneous thermalization of the sample is critical when the scattered signal itself is used as a thermometer to check the isothermal condition. The crystallization was initiated by cooling the sample temperature from 210 to 145 °C at the rate of 1.3 °C/s in about 50 s.

Simultaneous SAXS and WAXS measurements were carried out at the beam line ID2 of the European Synchrotron Radiation Facility (ESRF) in Grenoble, France [18]. The combined SAXS and WAXS experiments probed a wide scattering wave vector (q) range, $0.01\ \mathrm{nm}^{-1} \le q \le 25\ \mathrm{nm}^{-1}$, where $q = (4\pi/\lambda)\sin(\theta/2)$, with θ the scattering angle and λ the X-ray wavelength (≈ 1 Å). The SAXS detector was a high sensitivity fiber-optic coupled CCD (FReLoN) placed in an evacuated flight tube. The sample to SAXS detector distance was either 3 or 7 m. One sector of WAXS pattern was recorded simultaneously with SAXS by another detector (Micro Channel Plate image intensified CCD) positioned close to the sample (about 10 cm) [12]. The nominal intensity dynamic range of both SAXS and WAXS detectors is 2^{16} with the average single X-ray photon signal above the noise level of the CCD. The incident and transmitted intensities ($>10^{13}$ photons/s) were also simultaneously recorded. Using these intensities, measured two dimensional SAXS and WAXS patterns were normalized to an absolute scale and then azimuthally averaged to obtain the scattered intensity denoted by $I(q)$ which refers to the differential scattering cross-section per unit volume. The high incident intensity together with high sensitivity of SAXS and WAXS detectors provided a cumulative improvement of detectivity by several orders of magnitude. Complementary USAXS measurements were performed using a Bonse–Hart camera with crossed analyzer configuration [18].

SAXS and WAXS patterns were recorded from the beginning of the temperature quench and continuously after reaching the isothermal condition. Typical acquisition time was 0.2 s for both SAXS and WAXS and it was sufficient to record a set of frames at intervals of 5 s during the fast growth and 20 s at late stages (also to avoid any radiation damage to the sample). After reaching the crystallization temperature of 145 °C in about 50 s, SAXS and WAXS intensities monotonically decreased for another 10 s and then remained stable for about 20 s. This state of little variation of intensities was taken as isothermal condition and the corresponding intensities were used as the melt background for subsequent analysis. The isothermal time (t_{Iso}) evolved from this reference state. Both SAXS and WAXS at this stage have similar functional form as the corresponding melt patterns at 210 °C, except for a small decrease in their absolute intensity levels because of the change in temperature. It is important to note that the *induction period* strongly depends on the sensitivity of the experimental probe. For the high detectivity of SAXS and WAXS techniques employed here, the induction period has nearly diminished *albeit* similar crystallization condition as in previous studies [9–11].

3. Results and discussion

Fig. 1 shows the onset of the evolution of normalized SAXS and WAXS intensities from the initial isothermal level as a function of t_{Iso}. For better visibility, the melt background ($t_{Iso} = 0$ s) has been subtracted and each frame spans a range of azimuthal angle (90° and 40° for SAXS and WAXS,

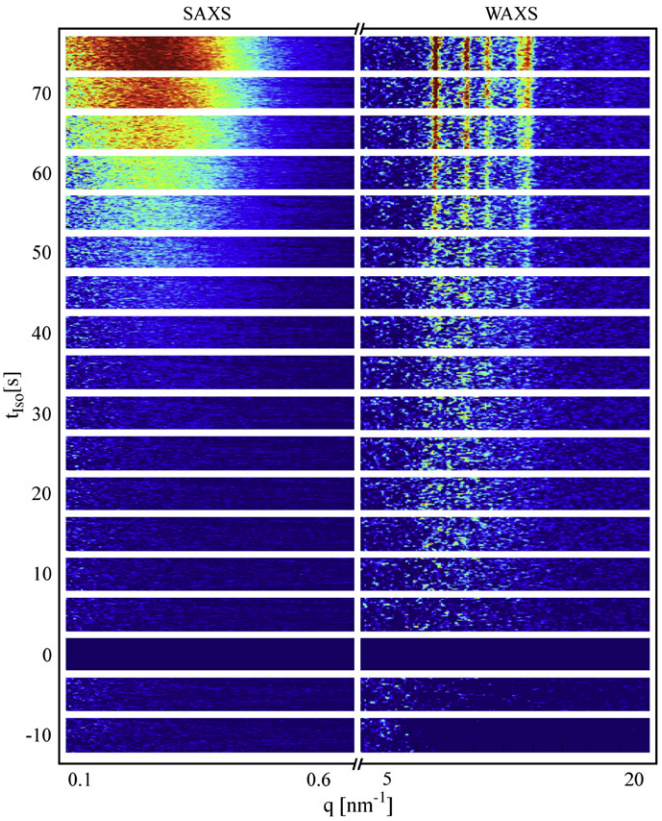

Fig. 1. Azimuthal sectors of SAXS and WAXS patterns recorded simultaneously following a rapid temperature quench to the crystallization temperature of 145 °C (t_{Iso} evolves after the sample reached the isothermal condition). The diffraction from crystalline (WAXS) nuclei is evident prior to significant evolution of SAXS.

respectively). The most striking feature of this plot is the clear evolution of WAXS signal prior to significant development of SAXS in contrast to previous experimental reports [9,11]. The initial WAXS intensity appeared as a relatively broad peak and the SAXS signal started to evolve noticeably with the emergence of sharp diffraction peaks in WAXS. This demonstrates that the previously reported evolution of SAXS intensity prior to the appearance of crystalline WAXS was very likely a consequence of the limited WAXS detectivity available in those studies [9,11]. In other words, crystalline nuclei have appeared prior to the spinodal-like evolution of initial SAXS intensity. This seriously challenges the hypothesis of spinodal-assisted mechanism for early stage of crystallization [7].

Fig. 2 depicts the azimuthally averaged SAXS intensity from the early stage of growth. For a comparison, corresponding unsubtracted intensity is presented as an inset. It is evident that the mesoscopic periodicity as represented by the broad peak in SAXS (q_{Max}) is well defined from the very early stages that could be similar to the smectic pearl state observed in computer simulations [3]. The functional form of $I(q)$ in Fig. 2 remains self-similar during the initial growth process. Fig. 3 presents the azimuthally averaged WAXS intensity from the early stage of growth. Corresponding unsubtracted intensity is shown as an inset. The diffraction peaks in WAXS are visible at the very early stage ($t_{Iso} > 30$ s) and

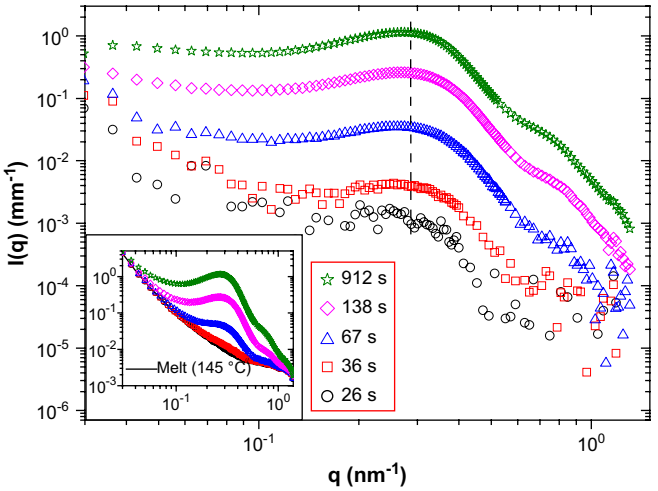

Fig. 2. Onset of SAXS intensity and its subsequent evolution as a function of t_{Iso} at 145 °C. The inset presents corresponding unsubtracted intensities together with the melt curve. The dotted line at q_{Max} indicates the constant mesoscopic periodicity of the lamellar structure during the growth process. The SAXS intensity detection limit for this specific instrument configuration was of the order of 3×10^{-6} mm^{-1}.

correspond to the α-monoclinic form of i-PP [11]. From the shape analysis of these Bragg reflections, the crystal size L_C can be estimated using the Scherrer relation, $L_C = 2\pi K/\Delta q_B$, where Δq_B is the full-width at half maximum of the Bragg peak and K is a constant depending on the shape of crystallites ($\approx$0.94 and 1.11 for cubic and spherical shapes, respectively) [19]. The line shape of principal reflections 110, 040 and 130 were analyzed using the Pearson VII function and the PeakFit program. The cumulative WAXS resolution for the specific configuration was about 0.3 nm^{-1} which limited the maximum crystal size that can be determined to about

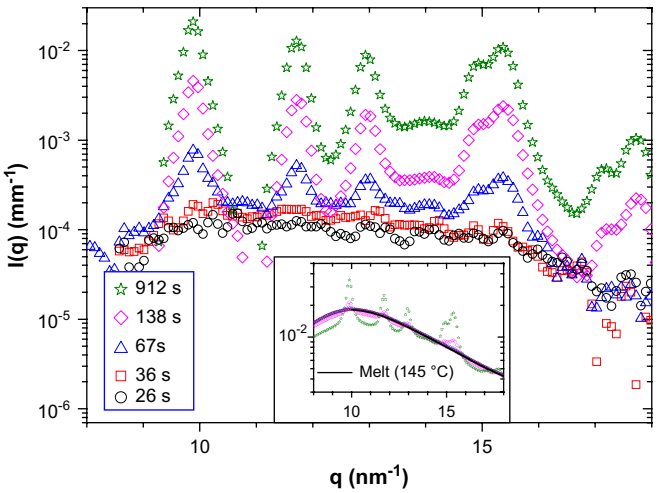

Fig. 3. Onset of WAXS intensity and its subsequent evolution as a function of t_{Iso} at 145 °C. The inset presents the corresponding unsubtracted intensities together with the melt curve. The crystalline peak positions become evident at 36 s and the main reflections correspond to 110, 040, 130, 111, 140 of the α-monoclinic phase. The WAXS intensity detection limit for this specific instrument configuration was of the order of 3×10^{-6} mm^{-1}.

20 nm. At $t_{Iso} = 50$ s, L_C was estimated to be 5 ± 1 nm and the resolution limit (20 nm) was reached at about $t_{Iso} = 100$ s.

To follow the growth kinetics, the scattering invariant (Q_I) and crystallinity (X_C) were calculated from the normalized SAXS and WAXS intensities, respectively. Here, Q_I is given by the relation, $Q_I = \int_{q_1}^{q_2} I(q)q^2 dq$, with $q_1 \approx 0.08$ nm^{-1} and $q_2 \approx 1.8$ nm^{-1} and this range corresponds to the most significant variation in SAXS intensity. The crystallinity is estimated from the ratio of the crystalline peak intensity (I_C) to the total intensity comprising the amorphous halo (I_A) and the crystalline peaks in the WAXS, $X_C = \int_{q_1}^{q_2} I_C(q)dq / \int_{q_1}^{q_2} (I_C(q) + I_A(q))dq$ with $q_1 \approx 5$ nm^{-1} and $q_2 \approx 16.5$ nm^{-1}. $I_A(q)$ is evaluated from the melt pattern immediately after reaching the isothermal condition ($t_{Iso} = 0$ s). The amorphous level at subsequent stages of growth was estimated by scaling the reference melt curve to the low q range of WAXS (5–6 nm^{-1}) where there is not significant contribution from the crystalline peaks [20]. Usually X_C is a better indicative of crystalline volume fraction while Q_I is a function of both amorphous and crystalline volume fractions (ϕ_A and ϕ_C, respectively). For a two-phase system consisting of amorphous and crystalline components, $Q_I = 2\pi^2(\rho_C^* - \rho_A^*)^2 \phi_C \phi_A$, where ρ_C^* and ρ_A^* are the scattering length densities of crystalline and amorphous regions.

The evolution of X_C and Q_I as a function of t_{Iso} is presented in Fig. 4. Qualitatively, both quantities follow an exponential type growth with $X_C = X_C(\infty)\{1 - \exp[-(t_{Iso} - t_I)/\tau_C]\}$, where $X_C(\infty)$ is the final value of X_C, t_I is an induction time, and $1/\tau_C$ is the growth rate. This expression is identical to the Avrami function conventionally used to describe crystallization kinetics [21]. An important feature in Fig. 3 is that the initial growths of X_C and Q_I significantly deviate from Avrami type behavior as shown in the inset. This initial level of X_C is primarily contributed by the broad peaks in the WAXS pattern observed prior to significant of evolution of SAXS. This plateau in crystallinity could be largely originating from the so-called baby nuclei observed in computer simulations [3]. In

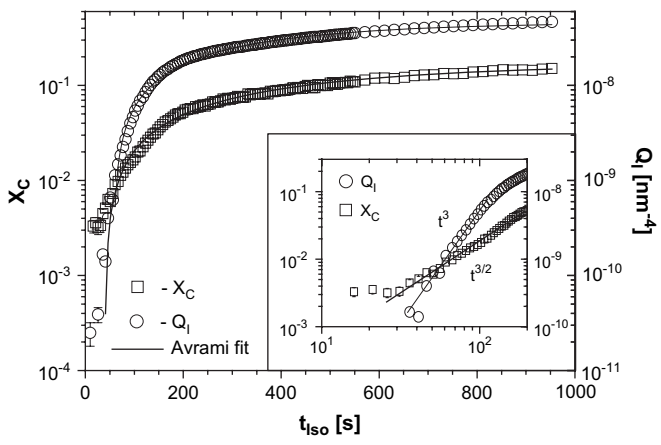

Fig. 4. Evolution of crystallinity and SAXS invariant during the early stages. The continuous lines show Avrami type growth kinetics with $n \approx 1$ and $\tau_C \approx 323$ and 486 s for SAXS and WAXS, respectively. The inset depicts power-law growth of X_C and Q_I after 30 s of reaching the isothermal condition. The error bars for X_C and Q_I are of the order of 5×10^{-4} and 6×10^{-12}, respectively.

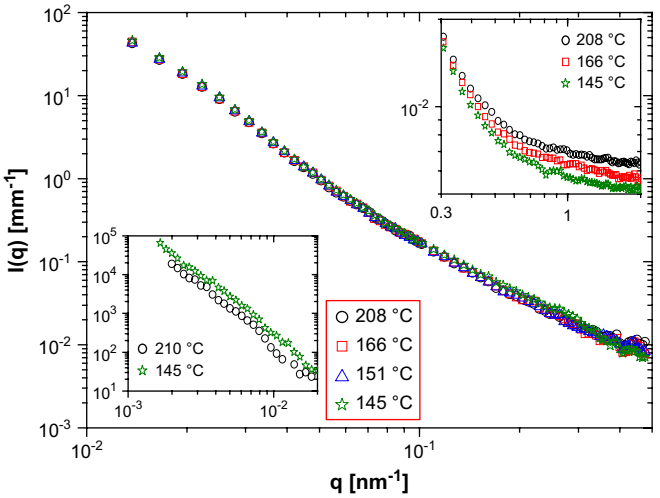

Fig. 5. Typical evolution of SAXS intensity during the temperature quench (1.33 °C/s) of the melt to the crystallization temperature at 145 °C. Upper and lower insets illustrate the corresponding changes at low and high q regions, respectively.

this metastable state, only the most favorable nuclei survive while nascent nuclei appear spontaneously resulting in a constant level of crystallinity ($t_{Iso} < 30$ s). This is not reflected in Q_I presumably due to the high q cut-off (1.8 nm^{-1}) used in the calculation. In the following step, X_C and Q_I grow by $t_{Iso}^{3/2}$ and t_{Iso}^3, respectively as depicted in the inset of Fig. 4. For constant thickness of lamellae, $X_C \propto t_{Iso}^{3/2}$ corresponds to a lateral growth by $t_{Iso}^{3/4}$ analogous to that seen in computer simulations [3]. The stronger time dependence of Q_I may be contributed by changes in interface scattering and melt density. The growth kinetics at subsequent stage is adequately described by the conventional Avrami function with exponent, $n \approx 1$. In reality, n depends on a whole host of parameters, in addition to the dimensionality of crystal growth as demonstrated by models involving cluster distribution rate equation [22]. This numerical analysis showed that the crystallization kinetics deviates from Avrami behavior both at initial and final stages. Furthermore, $n \approx 1$ implies high crystal nucleation rate and short induction period [22].

To further examine possible signature of long-range order parameter fluctuations as suggested by spinodal type mechanism, the evolution of SAXS intensity was monitored over a wider q range during the non-isothermal cooling. Fig. 5 presents the observed behavior at different q ranges. The lower inset of Fig. 5 shows the variation of $I(q)$ at very low q region. Clearly, there is not any spectacular feature in this ultra small-angle range as that would have been expected for a spinodal-assisted process except a constant shift due to change in density. This observation is consistent with the recent SANS study of polymer crystallization from solution [13]. On the other hand, $I(q)$ at high q range (upper inset of Fig. 5) decreased slightly which can be attributed to the lowering of the osmotic compressibility of the polymer melt. This further demonstrates that the dominant structural changes during the isothermal crystallization are captured in the SAXS and WAXS ranges presented in Figs. 2 and 3, respectively.

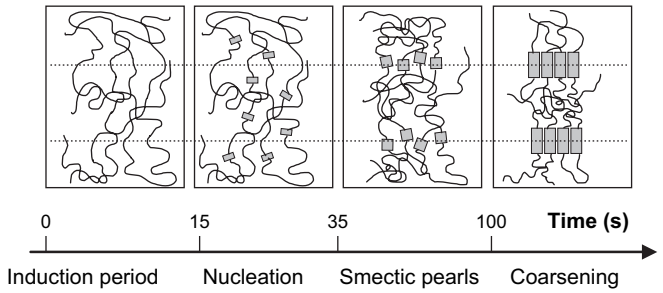

Fig. 6. Schematic representation of the different stages of nucleation and growth derived from the early stage SAXS/WAXS data. The dotted lines represent a constant mesoscopic periodicity of the lamellae as indicated by the q_{Max} in Fig. 2.

Fig. 6 summarizes the different stages of crystallization observed in this study. As illustrated by Figs. 1–3, the crystallinity appears much earlier than that observed in previous studies under identical conditions [9–11]. The limited detectivity of WAXS in those experiments (a few %) most likely led to the apparent evolution of SAXS prior to appearance of crystalline diffraction in WAXS. Although, the recent molecular dynamics simulation supported a spinodal-like structural development, the time scale of simulations and experiment are at least 10 orders of magnitude different [17]. Fig. 2 clearly demonstrates that the SAXS intensity has the same feature of that arising from the lamellar structure throughout the initial stages of growth. The early stage precursors reported by a recent dielectric spectroscopy study of polymer melt crystallization [23] may be explained on the basis of multiple baby nuclei at different segments of the same polymer chain [3]. In this way, the melt chain dynamics (probed by α relaxation) is modified prior to detectable crystalline structure development (β relaxation) [23].

4. Conclusions

In summary, the high detection capability of X-ray scattering techniques realized in this work allowed us to explore the very early stage of polymer crystallization that has not been accessed in previous studies. Over this unexplored time window of crystallization kinetics, we have observed the initial nucleation and growth of crystalline moieties prior to significant evolution of SAXS intensity. In addition, there is no signature of long-range density fluctuations supporting spinodal decomposition like mechanism for polymer crystallization. In conclusion, the early stage of isothermal crystallization in isotactic polypropylene is adequately described by nucleation and growth mechanism.

Acknowledgements

We thank A. Mahendrasingam (Keele University, U.K.) for kindly providing i-PP samples and W.H. De Jeu (FOM, Amsterdam) for useful discussions. The European Synchrotron Radiation Facility is acknowledged for the provision of beam time.

References

[1] Mandelkern L. Biophys Chem 2004;112:109.
[2] Keller A, Cheng SZD. Polymer 1998;39:4461.
[3] Muthukumar M. Philos Trans R Soc A 2003;361:539;
Adv Polym Sci 2005;191:241.
[4] Strobl G. Eur Phys J E 2000;3:165.
[5] Hoffman JD, Davis GT, Lauritzen JI. In: Hannay NB, editor. Treatise on solid state chemistry, vol. 3. New York: Plenum; 1976. p. 497.
[6] Kaji K, Nishida K, Kanaya T, Matsuba G, Konishi T, Imai M. Adv Polym Sci 2005;191:187.
[7] Olmsted PD, Poon WCK, McLeish TC, Terrill NJ, Ryan AJ. Phys Rev Lett 1998;81:373.
[8] Imai M, Kaji K, Kanaya T. Phys Rev Lett 1993;71:4162.
[9] Terrill NJ, Fairclough PA, Towns-Andrews E, Komanschek BU, Young RJ, Ryan AJ. Polymer 1998;39:2381.
[10] Wang ZG, Hsiao BS, Sirota E, Agarwal P, Srinivas S. Macromolecules 2000;33:978.
[11] Heeley EL, Maidens A, Olmsted PD, Bras W, Dolbnya IP, Fairclough JPA, et al. Macromolecules 2003;36:3656.
[12] Panine P, Urban V, Boesecke P, Narayanan T. J Appl Crystallogr 2003;36:991.
[13] Wang H. Polym Commun 2006;47:4897.
[14] Kawakami D, Hsiao BS, Burger C, Ran S, Avila-Orta C, Sics I, et al. Macromolecules 2005;38:91.
[15] Mahendrasingam A, Blundell DJ, Martin C, Urban V, Narayanan T, Fuller W. Polymer 2005;46:6044.
[16] Li LB, de Jeu WH. Phys Rev Lett 2004;92:075506;
See also Byelov D, Panine P, de Jeu WH. Macromolecules 2007;40:288.
[17] Gee RH, Lacevic N, Fried LE. Nature Materials 2006;5:39.
[18] Narayanan T, Diat O, Boesecke P. Nuclear Instrum Meth Phys Res A 2001;467–468:1005.
[19] Patterson AL. Phys Rev 1939;56:978.
[20] Chung FH, Scott RW. J Appl Crystallogr 1973;6:225.
[21] Avrami M. J Chem Phys 1939;7:1103.
[22] Yang J, McCoy BJ, Madras G. J Chem Phys 2005;122:064901.
[23] Soccio M, Nogales A, Lotti N, Munari A, Ezquerra TA. Phys Rev Lett 2007;98:037801.